Anti-Jamming Multi-Target Parameter Estimation Using Space-Time Cascaded Adaptive Monopulse

Ling QIAO [1], Mingwei SHEN [2], Ruiyan CHEN [1], Yongshu ZHANG [1], Di WU [3], Daiyin ZHU [3]

[1] College of Information Science and Engineering, Hohai University, No. 1915 Hohai Avenue, Changzhou, 213200, China
[2] College of Computer Science and Software Engineering, Hohai University, No. 8 Focheng West Road, Nanjing, 211100, China
[3] Key Laboratory of Radar Imaging and Microwave Photonics, Ministry of Education, Nanjing University of Aeronautics and Astronautics, No. 29 Jiangjun Avenue, Nanjing, 211106, China

230223080005@hhu.edu.cn, smw_hhu1981@163.com, c1929995841@163.com, 211307010013@hhu.edu.cn, wudi82@nuaa.edu.cn, zhudy@nuaa.edu.cn

Submitted December 30, 2025 / Accepted May 8, 2026 / Online first May 26, 2026

Abstract. *The multi-target space-time cascaded monopulse (M-STCMP) algorithm is an efficient method for parameter estimation in radar systems. However, under jamming conditions, the signal-to-jamming-plus-noise ratio (SJNR) deteriorates significantly, causing the sum and difference beam weights computed by the M-STCMP algorithm to become unreliable for target parameter estimation. To address this limitation, this paper proposes an anti-jamming multi-target space-time cascaded monopulse (AM-STCMP) algorithm as a robust framework for multi-target parameter estimation. The proposed AM-STCMP algorithm improves the conventional M-STCMP framework by integrating spatial adaptive monopulse processing. Unlike conventional derivative-based methods, this approach adaptively optimizes the sum and difference beam weights through maximum likelihood estimation, thereby effectively suppressing strong jamming while maintaining estimation accuracy. In addition, iterative optimization of the angle discrimination curve enhances the SJNR and improves parameter estimation accuracy. In the subsequent processing stage, the algorithm employs space-time cascaded monopulse processing for efficient range-velocity estimation and uses the RELAX algorithm for high-precision angle-velocity-range estimation, thereby maintaining accuracy while reducing computational complexity. Theoretical analysis and Monte Carlo simulations validate the AM-STCMP algorithm and demonstrate its improved robustness under strong jamming conditions.*

Keywords

Spatial adaptive monopulse, space-time cascaded monopulse, jamming suppression, three-dimensional parameter estimation

1. Introduction

Monopulse angle measurement is an effective technique for target direction estimation and generally has lower computational complexity than the MUSIC algorithm [1–3]. However, monopulse radar cannot distinguish between target sets located within the same range-Doppler cell. As a result, the estimation is affected by the energy center of the target sets [4]. To improve the angle estimation performance of monopulse radar in multi-target environments, researchers have made extensive efforts in this direction.

In 1971, Sherman used the complex ratio of the sum and difference signals formed from two pulses to estimate the angles of two targets, thereby laying the foundation for multi-target detection using monopulse radar [5]. Subsequently, several methods have been proposed, including moment-matching, maximum-likelihood, and four-channel closed-form angle estimation methods. However, these algorithms are typically limited to scenarios involving only two targets [6–8]. To overcome this limitation, several extended methods have been proposed, including the approximate maximum-likelihood relaxation estimation method, the joint Doppler-angle maximum-likelihood estimation method, and the amplitude comparison monopulse-maximum likelihood (ACM-ML) method [9–11]. Nevertheless, these methods rely on joint maximum-likelihood estimation, which requires two-dimensional iterative optimization and leads to high computational complexity, making real-time processing difficult [12]. In [13], a time-domain monopulse velocity measurement algorithm was introduced to accelerate the two-dimensional ML search in the ACM-ML algorithm. In addition, an efficient multi-target parameter estimation algorithm based on space-time cascaded monopulse processing, referred to as the M-STCMP algorithm, was proposed. However, the angle measurement algorithm employed in this approach still relies on the conventional monopulse method. In jamming-prone environments, antenna pattern distortion

DOI: 10.13164/re.2026.0323

can significantly degrade the algorithm's estimation performance. To improve the anti-jamming performance of monopulse angle measurement, adaptive digital beamforming (ADBF) has been introduced to achieve high-precision angle estimation in jamming environments.

ADBF is a spatial filtering technique that forms nulls in the directions of jamming sources, thereby enhancing the desired signal output while suppressing jamming. When integrated with monopulse angle measurement, ADBF can effectively reduce the impact of jamming on angle estimation and enable high-precision measurements in jamming-prone environments [14]. Since Van Atta first proposed adaptive array processing in 1959, researchers have sought to improve this technique in terms of array signal processing performance, data processing speed, and application scope. In this context, various algorithms have been proposed, such as the least mean square (LMS) and recursive least squares (RLS) algorithms [15], [16]. An adaptive beamforming method for broadening jamming nulls was introduced in [17]. This method is easy to implement and can effectively suppress jamming even when the jammer direction changes. In 2022, Xiong and Xie [18] proposed a two-dimensional hierarchical adaptive monopulse beamforming algorithm, which jointly suppresses both main lobe and sidelobe jamming by hierarchically processing angular and orthogonal dimensions, thereby ensuring high-accuracy angle measurement.

This paper proposes an anti-jamming multi-target parameter estimation algorithm based on space-time cascaded monopulse processing. The proposed method extends the work in [13] by introducing spatial adaptive monopulse angle measurement into the M-STCMP framework. In the proposed algorithm, spatial adaptive monopulse correction is applied to the sum and difference weight vectors to mitigate the impact of jamming signals in radar echoes. This enhancement improves the anti-jamming capability of the M-STCMP algorithm and enables accurate three-dimensional parameter estimation of each target, including velocity, range, and angle.

2. Basic Principle of the M-STCMP

Consider a linear array with N_e elements, where the spacing d between adjacent elements is assumed to be much larger than the physical size of each antenna element. A chirp signal is transmitted, and all signals are assumed to be far-field and narrowband. The target signal is incident on the antenna array at an angle θ.

The angle estimate can be expressed as [11]:

$$\hat{\theta} = \theta' + \frac{1}{k}\mathrm{Re}\left(\frac{\omega_\Delta^{\mathrm{H}}\mathbf{a}(\theta)}{\omega_\Sigma^{\mathrm{H}}\mathbf{a}(\theta)}\right) = \theta' + \frac{1}{k}\mathrm{Re}\left(\frac{\mathbf{G}_\Delta(\theta)}{\mathbf{G}_\Sigma(\theta)}\right) \quad (1)$$

where θ' represents the angle observation value; $\mathbf{a}(\theta)$ represents the array steering vector; the sum and difference beam weight vectors are $\boldsymbol{\omega}_\Sigma = \mathbf{a}(\theta)$ and $\boldsymbol{\omega}_\Delta = \mathrm{d}\boldsymbol{\omega}_\Sigma/\mathrm{d}\theta$, respectively; $\mathbf{G}_\Delta(\theta)$ and $\mathbf{G}_\Sigma(\theta)$ denote the difference and sum beam amplitude gains, respectively; k represents the slope of the monopulse ratio in the spatial domain; $\mathrm{Re}(\cdot)$ represents the real part of the complex quantity; the superscript $(\cdot)^{\mathrm{H}}$ denotes the conjugate transpose.

The velocity estimate can be expressed as [19]:

$$\hat{v} = v' + \frac{\mathbf{w}_\Delta^{\mathrm{H}}\mathbf{s}(v)}{\mathbf{w}_\Sigma^{\mathrm{H}}\mathbf{s}(v)}\Big/k_v = v' + \frac{\mathbf{Y}_{v,\Delta}}{\mathbf{Y}_{v,\Sigma}}\Big/k_v \quad (2)$$

where v' is the velocity observation value; $\mathbf{s}(v)$ is the temporal steering vector; the sum and difference beam weight vectors are $\mathbf{w}_\Sigma = \mathbf{s}(v)$ and $\mathbf{w}_\Delta = \mathrm{d}\mathbf{w}_\Sigma/\mathrm{d}v$, respectively; $\mathbf{Y}_{v,\Delta}$ and $\mathbf{Y}_{v,\Sigma}$ are the sum and difference beam gains, respectively; and k_v represents the slope of the temporal monopulse ratio.

When multiple targets are present in the scenario, an improved RELAX algorithm is employed for multi-target parameter estimation. After fast Fourier transform (FFT) processing of the received data, the N targets are assumed to be distributed across K Doppler cells. When the targets are clustered within the same Doppler cell, K is equal to 1. The sum and difference channel outputs of the nth target in the kth Doppler cell can subsequently be expressed as follows:

$$\mathbf{Y}_\Sigma^{(k,n)} = \mathbf{Y}_\Sigma - \sum_{l=1,l\neq n}^{N_k} \hat{\alpha}^{(l)}\mathbf{Z}^{(l)}(\hat{r}^{(l)}, \hat{v}^{(l)}), \quad (3)$$

$$\mathbf{Y}_\Delta^{(k,n)} = \mathbf{Y}_\Delta - \sum_{l=1,l\neq n}^{N_k} \hat{\beta}^{(l)}\mathbf{Z}^{(l)}(\hat{r}^{(l)}, \hat{v}^{(l)}) \quad (4)$$

where $k = 1, 2, \ldots, K$, N_k represents the number of targets in the kth Doppler cell; $\mathbf{Y}_\Sigma$ represents the sum channel output of the N targets and noise; $\mathbf{Y}_\Delta$ represents the difference channel output of the N targets and noise; and $[\hat{v}_n^{(l)}, \hat{r}_n^{(l)}, \hat{\alpha}_n^{(l)}, \hat{\beta}_n^{(l)}]_{n\in[1,N],l\neq n}$ represents the velocity, range, sum channel amplitudes and difference channel amplitudes of the remaining N–1 components. $\mathbf{Z}$ is the reconstructed matrix of outputs from the remaining N–1 components.

Performing the inverse fast Fourier transform (IFFT) on (3) yields the corresponding temporal output. Substituting this result into (2) provides the estimated velocity $v^{(k,n)}$. The remaining parameters $[\alpha^{(k,n)}, \beta^{(k,n)}, \theta^{(k,n)}]$ are obtained according to [13].

The remaining component of the lth iteration is defined as:

$$\mathbf{C}^{(l)} = \mathbf{I}\cdot\left|\mathbf{Y}_\Sigma^{(k,n)} - \sum_{n=1}^{n}\hat{\alpha}^{(k,n)}\mathbf{Z}^{(k,n)}\left(\hat{r}^{(k,n)}, \hat{v}^{(k,n)}\right)\right|. \quad (5)$$

Let $\mathbf{I}$ denote an all-one vector. The iteration is terminated when the number of iterations reaches the predefined maximum or when the rate of change in the residual components between the lth and (l+1)th iterations falls below a specified threshold. Finally, all target parameters are jointly refined by the RELAX iteration, yielding more accurate parameter estimates [13].

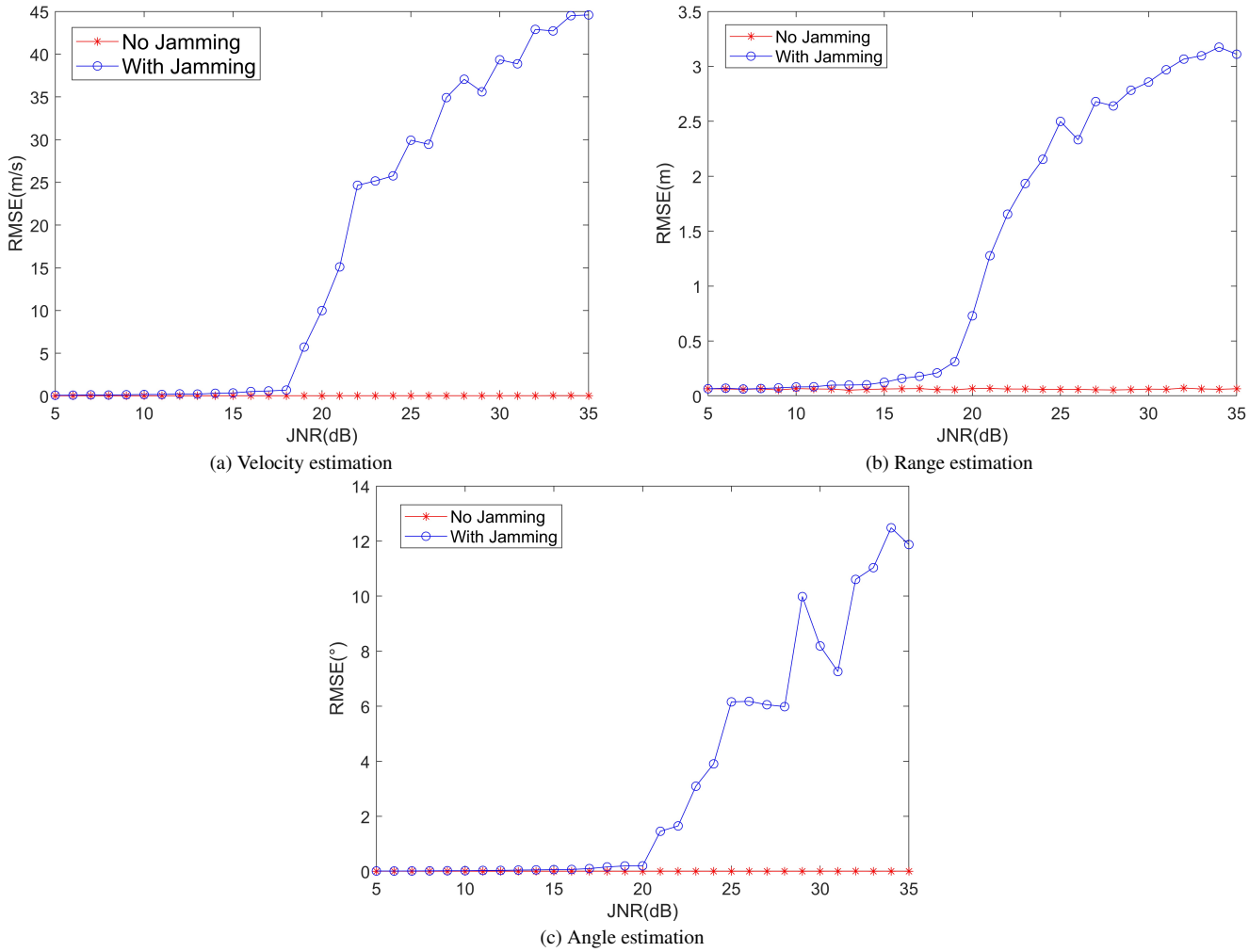

(a) Velocity estimation

(b) Range estimation

(c) Angle estimation

Fig. 1. The impact of jamming on the performance of M-STCMP.

Compared with the maximum likelihood-based multi-parameter joint search methods, the M-STCMP algorithm significantly reduces the computational complexity. However, in jamming-prone environments, the estimation performance of the algorithm degrades considerably. Figure 1 illustrates the impact of jamming on the velocity, range, and angle estimation performance of the M-STCMP algorithm. To further emphasize the effect of jamming, the jammer direction is set to 5°, close to the main lobe. The target velocity is 27.9 m/s, the range is 351.2 m, the angle is 0.5°, the signal-to-noise ratio (SNR) is set to 20 dB, and the number of Monte Carlo simulations is 100. As shown in Fig. 1, jamming significantly affects the performance of the M-STCMP algorithm. Specifically, when the jamming-to-noise ratio (JNR) is relatively low, jamming has minimal impact on parameter estimation performance; however, as the JNR increases, the root mean square error (RMSE) values of all three parameter estimates increase. To address the degradation caused by jamming, this paper introduces spatial adaptive monopulse processing into the M-STCMP algorithm to enhance anti-jamming capability, thereby forming the proposed AM-STCMP algorithm.

3. AM-STCMP Algorithm

3.1 Adaptive Monopulse Principle

When the target is located within the linear region of the monopulse response, the main lobe of the radar antenna pattern is steered toward the observation angle. To facilitate the parabolic approximation used for maximum-likelihood angle estimation, the following objective function is defined [20]:

$$F(u) = \log\left[S_{\text{scan}}(u)\right] \tag{6}$$

where $u = \sin\theta$, θ represents the observation angle of the scanning antenna, and θ_0 is the true angle value of the target. Here, $S_{\text{scan}}(u)$ denotes the scan power pattern associated with the sum beam steered to the trial spatial direction u. It is defined as

$$S_{\text{scan}}(u) = \left|\mathbf{w}_S^{\text{H}}(u)\mathbf{z}\right|^2 = \frac{\left|\mathbf{a}^{\text{H}}(u)\mathbf{Q}^{-1}\mathbf{z}\right|^2}{\mathbf{a}^{\text{H}}(u)\mathbf{Q}^{-1}\mathbf{a}(u)}$$

where $\mathbf{w}_S(u)$ is the direction-dependent sum-beam weight vector used in the scan pattern, $\mathbf{z}$ is the received data

vector, $\mathbf{a}(u)$ is the steering vector parameterized by u, and $\mathbf{Q}$ is the positive-definite matrix used in the maximum-likelihood scan formulation. When the scanning angle θ coincides with the true target angle θ_0 ($\theta = \theta_0$), $F(u)$ reaches its maximum value, and the maximum-likelihood solution θ_{ML} at this point is used as the updated value for iteration. Performing a first-order Taylor expansion of $F_u(u)$ at θ_0 yields:

$$F_u(u_{\mathrm{ML}}) = F_u(u_0) + F_{uu}(u_0)(u_{\mathrm{ML}} - u_0) \tag{7}$$

where $u_{\mathrm{ML}} = \sin\theta_{\mathrm{ML}}$, the subscript u represents the first derivative and the subscript uu represents the second derivative. When the observation angle approaches the target angle, it can be approximately considered that $F_{uu}(u_0) = F_{uu}(u_{\mathrm{ML}})$. Additionally, at point θ_0, $F_u(u_0) = 0$. Therefore, Equation (7) can be rewritten as:

$$u_0 = u_{\mathrm{ML}} - F_{uu}(u_{\mathrm{ML}})^{-1} F_u(u_{\mathrm{ML}}). \tag{8}$$

In the conventional monopulse algorithm, $\mathbf{Q}$ is the identity matrix $\mathbf{I}$, whereas in the adaptive monopulse algorithm, $\mathbf{Q}$ is the estimated jamming-plus-noise covariance matrix. Therefore, the correction factor is as follows:

$$\mu_x = \mathrm{Re}\left\{\frac{\mathbf{a}_u^{\mathrm{H}}\mathbf{Q}^{-1}\mathbf{a}}{\mathbf{a}^{\mathrm{H}}\mathbf{Q}^{-1}\mathbf{a}}\right\}. \tag{9}$$

$F_u(u)$ and $F_{uu}(u)$ are expressed as follows [20]:

$$F_u = \frac{(S_{\mathrm{scan}})_u}{S_{\mathrm{scan}}} = 2\mathrm{Re}\left\{\frac{\mathbf{w}_{\mathrm{D}}^{\mathrm{H}}\mathbf{z}}{\mathbf{w}_{\mathrm{S}}^{\mathrm{H}}\mathbf{z}}\right\} - 2\mu_x, \tag{10}$$

$$F_{uu} = 2\mu_x^2 - 2\frac{\mathbf{w}_{\mathrm{D}}^{\mathrm{H}}\mathbf{a}_u(u)}{\mathbf{w}^{\mathrm{H}}\mathbf{a}(u)} \tag{11}$$

where $\mathbf{w}$ denotes the beamforming weight vector, and $\mathbf{w}_{\mathrm{S}}$ and $\mathbf{w}_{\mathrm{D}}$ represent the weights of the adaptive sum and difference beams, respectively. $\mathbf{z}$ is the received data. Substituting u_{ML}, $F_u(u_{\mathrm{ML}})$ and $F_{uu}(u_{\mathrm{ML}})$ into (8) yields the angle θ_0 of the target. To further improve the accuracy of the angle measurement, the above process can be iterated, and the estimated value after k iterations is

$$\theta^{(k+1)} = \theta^{(k)} - F_{\theta\theta}(\theta^{(k)})^{-1} F_\theta(\theta^{(k)}). \tag{12}$$

Figures 2 and 3 present the simulated adaptive sum and difference antenna patterns, as well as the angle discrimination curves, respectively. The array has 21 elements, and the element spacing-to-wavelength ratio is 1/2. The jamming angle is set at 6°, and the initial target iteration value is 0°. As shown in Fig. 2, the adaptive sum beam forms a main lobe at the target angle, whereas the difference beam creates a null at the same angle. Both the sum and difference beams produce nulls in the jamming angle. As demonstrated in Fig. 3, the adaptive monopulse technique maintains nearly linear characteristics in its angle discrimination curve within the main lobe region under jamming conditions, exhibiting significant improvements over conventional angle discrimination curves. Thus, the adaptive monopulse can simultaneously suppress jamming and generate a beam directed at the target angle.

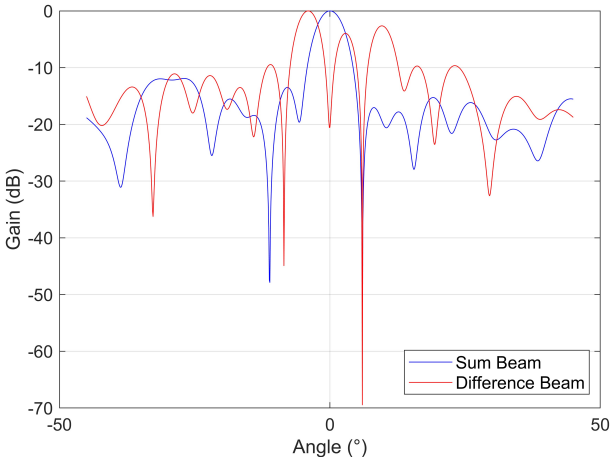

Fig. 2. Adaptive sum and difference beam antenna pattern.

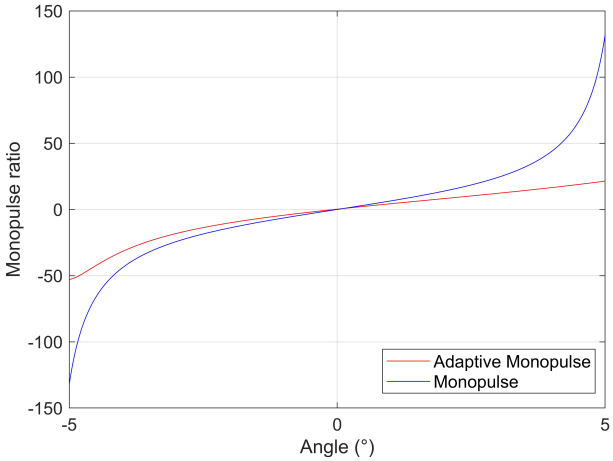

Fig. 3. Adaptive angle discrimination curve.

3.2 AM-STCMP Algorithm Principle

Under jamming conditions, the conventional derivative-based method for constructing the sum and difference beam weights becomes inadequate because it cannot maintain optimal performance in the presence of strong jamming signals. Therefore, the spatial adaptive monopulse algorithm from Sec. 3.1 is employed to construct the sum and difference beams. The received signal at the array elements can be expressed as:

$$\begin{aligned}\mathbf{x} &= \mathbf{s}^{(n)}(t_m, \hat{t})\mathbf{a}(\theta) + \mathbf{J} \\ &= \mathbf{A}^{(n)}\mathbf{s}(t - \tau_m^{(n)}) \exp\left[\mathrm{j}2\pi f_c \tau_m^{(n)}\right]\mathbf{a}(\theta) + \mathbf{J}\end{aligned} \tag{13}$$

where $\hat{t} = t - t_m$ is the fast-time variable, t denotes the duration, $t_m = mT_{\mathrm{r}}$ is the slow-time variable, and m denotes the pulse index of the linear frequency-modulated (LFM) signal. In addition, $\mathbf{a}(\theta)$ is the steering vector, θ is the target angle, $\mathbf{A}^{(n)}$ is the received signal amplitude of the nth target, $\tau_m^{(n)}$ is the delay of the nth target with respect to the mth pulse, and $\mathbf{J}$ denotes the jamming-plus-noise component. The received signal $\mathbf{x}$ is processed using FFT. Using a noise threshold, the received signal $\mathbf{x}$ is separated into two components: the signal vector $\mathbf{z}_{\mathrm{c}}$ and the jamming-plus-noise matrix $\mathbf{C}$. Based on these separated components, the spatial covariance matrix is subsequently derived as follows:

$$\mathbf{Q}_{\mathrm{c}} = \frac{1}{L}\sum_{l=0}^{L-1}\mathbf{C}\mathbf{C}^{\mathrm{H}} \tag{14}$$

where L is the number of samples used to estimate the covariance matrix. Therefore, the adaptive sum beam weight vector can be expressed as:

$$\mathbf{w}_{\mathrm{cp}}(\theta) = \left[\mathbf{a}(\theta)^{\mathrm{H}}\mathbf{Q}_{\mathrm{c}}^{-1}\mathbf{a}(\theta)\right]^{-\frac{1}{2}}\mathbf{Q}_{\mathrm{c}}^{-1}\mathbf{a}(\theta). \tag{15}$$

A function $F(u) = \log\left[S_{\mathrm{scan}}(u)\right]$ is constructed, where $u = \sin(\theta)$, and its first-order derivative is given as:

$$F_u = 2\mathrm{Re}\left\{\frac{\mathbf{w}_{\mathrm{D}}^{\mathrm{H}}\mathbf{z}_{\mathrm{c}}}{\mathbf{w}_{\mathrm{cp}}^{\mathrm{H}}\mathbf{z}_{\mathrm{c}}}\right\} - 2\mathrm{Re}\left\{\frac{\mathbf{a}_u^{\mathrm{H}}\mathbf{Q}_{\mathrm{c}}^{-1}\mathbf{a}}{\mathbf{a}^{\mathrm{H}}\mathbf{Q}_{\mathrm{c}}^{-1}\mathbf{a}}\right\}. \tag{16}$$

The second-order derivative can be expressed as:

$$F_{uu} = 2\left(\mathrm{Re}\left\{\frac{\mathbf{a}_u^{\mathrm{H}}\mathbf{Q}_{\mathrm{c}}^{-1}\mathbf{a}}{\mathbf{a}^{\mathrm{H}}\mathbf{Q}_{\mathrm{c}}^{-1}\mathbf{a}}\right\}\right)^2 - 2\frac{\mathbf{w}_{\mathrm{cm}}^{\mathrm{H}}\mathbf{a}_u(u)}{\mathbf{w}_{\mathrm{cp}}^{\mathrm{H}}\mathbf{a}(u)} \tag{17}$$

where $\mathbf{w}_{\mathrm{cm}}$ is the weight vector of the adaptive difference beam, which can be expressed as:

$$\mathbf{w}_{\mathrm{cm}} = \left(\mathbf{a}^{\mathrm{H}}\mathbf{Q}_{\mathrm{c}}^{-1}\mathbf{a}\right)^{-\frac{1}{2}}\mathbf{Q}_{\mathrm{c}}^{-1}\mathbf{a}_u. \tag{18}$$

After multiple iterations of the above equation, the initial angle observation θ_{c} is obtained. Substituting it into (15) and (18) yields the final sum and difference weights $\mathbf{w}_{\mathrm{S}}$ and $\mathbf{w}_{\mathrm{D}}$, respectively. Therefore, the modified sum channel output by the ADBF algorithm can be written as:

$$\begin{aligned}\mathbf{y}_{\Sigma}^{(n)} &= \mathbf{w}_{\mathrm{S}}^{\mathrm{H}}\mathbf{x}\\ &= \mathbf{G}_{\mathrm{S}}^{(n)}(\theta^{(n)})\mathbf{s}(t-\hat{\tau}_m^{(n)})\exp[\mathrm{j}2\pi f_{\mathrm{c}}\tau_m^{(n)}] + \mathbf{N}_{\Sigma}.\end{aligned} \tag{19}$$

The difference channel output is as follows:

$$\begin{aligned}\mathbf{y}_{\Delta}^{(n)} &= \mathbf{w}_{\mathrm{D}}^{\mathrm{H}}\mathbf{x}\\ &= \mathbf{G}_{\mathrm{D}}^{(n)}(\theta^{(n)})\mathbf{s}(t-\hat{\tau}_m^{(n)})\exp[\mathrm{j}2\pi f_{\mathrm{c}}\tau_m^{(n)}] + \mathbf{N}_{\Delta}\end{aligned} \tag{20}$$

where $\mathbf{N}_{\Sigma}$ and $\mathbf{N}_{\Delta}$ represent the residual noise components in the sum and difference channels after jamming suppression, respectively. At this stage, the jamming signals have been effectively suppressed, and the M-STCMP algorithm is subsequently employed to estimate the parameters as follows:

$$\hat{v}^{(n)} = v_0^{(n)} + \frac{1}{k_v}\frac{\mathbf{y}_{\Delta}^{(n)}}{\mathbf{y}_{\Sigma}^{(n)}}, \tag{21}$$

$$\hat{r}^{(n)} = \arg\max_{r}\frac{\left|\mathbf{Y}_{\Sigma}^{(n)}\mathbf{M}^{-1}[\mathbf{Z}^{(n)}(r,\hat{v}^{(n)})]\right|^2}{\mathbf{Z}(r,\hat{v}^{(n)})_{\Sigma}^{(n)}\mathbf{M}^{-1}[\mathbf{Z}^{(n)}(r,\hat{v}^{(n)})]^{\mathrm{H}}}, \tag{22}$$

$$\hat{\alpha}^{(n)} = \frac{\mathbf{Y}_{\Sigma}^{(n)}\mathbf{M}^{-1}[\mathbf{Z}^{(n)}(\hat{r}^{(n)},\hat{v}^{(n)})]^{\mathrm{H}}}{\mathbf{Z}(\hat{r}^{(n)},\hat{v}^{(n)})_{\Sigma}^{(n)}\mathbf{M}^{-1}[\mathbf{Z}^{(n)}(\hat{r}^{(n)},\hat{v}^{(n)})]^{\mathrm{H}}}, \tag{23}$$

$$\hat{\beta}^{(n)} = \frac{\mathbf{Y}_{\Delta}^{(n)}\mathbf{M}^{-1}[\mathbf{Z}^{(n)}(\hat{r}^{(n)},\hat{v}^{(n)})]^{\mathrm{H}}}{\mathbf{Z}(\hat{r}^{(n)},\hat{v}^{(n)})_{\Delta}^{(n)}\mathbf{M}^{-1}[\mathbf{Z}^{(n)}(\hat{r}^{(n)},\hat{v}^{(n)})]^{\mathrm{H}}} \tag{24}$$

where $\mathbf{Y}_{\Sigma}^{(n)}$ and $\mathbf{Y}_{\Delta}^{(n)}$ represent the frequency-domain forms of $\mathbf{y}_{\Sigma}^{(n)}$ and $\mathbf{y}_{\Delta}^{(n)}$, respectively; $\mathbf{M}$ denotes the time-domain covariance matrix; and $\mathbf{Z}$ corresponds to the matrix form of the original received signal. Since the signal model employed in this study is based on a far-field jamming model, jamming affects only the spatial covariance matrix $\mathbf{Q}_{\mathrm{c}}$, while the temporal covariance matrix $\mathbf{M}$ remains unaffected. As derived from (16), the first-order derivative is equivalent to the difference-to-sum ratio minus a correction term. Consequently, by substituting (23) and (24) into (16), we obtain the following result:

$$F_u^{(n)} = 2\,\mathrm{Re}\left\{\frac{\hat{\beta}^{(n)}}{\hat{\alpha}^{(n)}}\right\} - 2\,\mathrm{Re}\left\{\frac{\mathbf{a}_u^{\mathrm{H}}\mathbf{Q}_{\mathrm{c}}^{-1}\mathbf{a}}{\mathbf{a}^{\mathrm{H}}\mathbf{Q}_{\mathrm{c}}^{-1}\mathbf{a}}\right\}. \tag{25}$$

Therefore, the sine of the angle estimate is

$$\hat{u}^{(n)} = u_c - F_{uu}\left(\hat{u}^{(n)}\right)^{-1}F_u\left(u_c\right) \tag{26}$$

where $\hat{u}^{(n)} = \sin\hat{\theta}^{(n)}$, and u_c is the sine value of the maximum likelihood solution of the ADBF algorithm.

The flowchart of the proposed AM-STCMP algorithm is shown in Fig. 4, and its main steps are summarized as follows:

Step 1:

(1) Perform an FFT on the array received signal $\mathbf{x}$, and use noise thresholding to separate the signal $\mathbf{z}_{\mathrm{c}}$ and jamming-plus-noise matrix $\mathbf{C}$.

(2) Substitute $\mathbf{C}$ into (14) to obtain the spatial covariance matrix $\mathbf{Q}_{\mathrm{c}}$. By substituting $[\mathbf{x}, \mathbf{z}_{\mathrm{c}}, \mathbf{Q}_{\mathrm{c}}]$ into (15)–(18) and performing multiple iterations, the adaptive sum and difference weights $\mathbf{w}_{\mathrm{S}}$ and $\mathbf{w}_{\mathrm{D}}$ can be obtained, along with the initial angle observation value θ_{c}.

(3) Using the adaptive weights $[\mathbf{w}_{\mathrm{S}}, \mathbf{w}_{\mathrm{D}}]$ corrected by the ADBF, the sum and difference channel gains are obtained. Substituting them into (19) and (20) yields the sum and difference channel outputs $\mathbf{y}_{\Sigma}$ and $\mathbf{y}_{\Delta}$, respectively.

Step 2:

Based on the FFT result of $\mathbf{y}_{\Sigma}$, the data are separated into K Doppler-cell components, denoted by $\mathbf{x}_{\Sigma}^{(A)}$, $\mathbf{x}_{\Sigma}^{(B)}$, $\cdots$, $\mathbf{x}_{\Sigma}^{(K)}$, with the corresponding initial velocities $v_0^{(A)}$, $v_0^{(B)}$, $\cdots$, $v_0^{(K)}$. The components are ordered in descending energy.

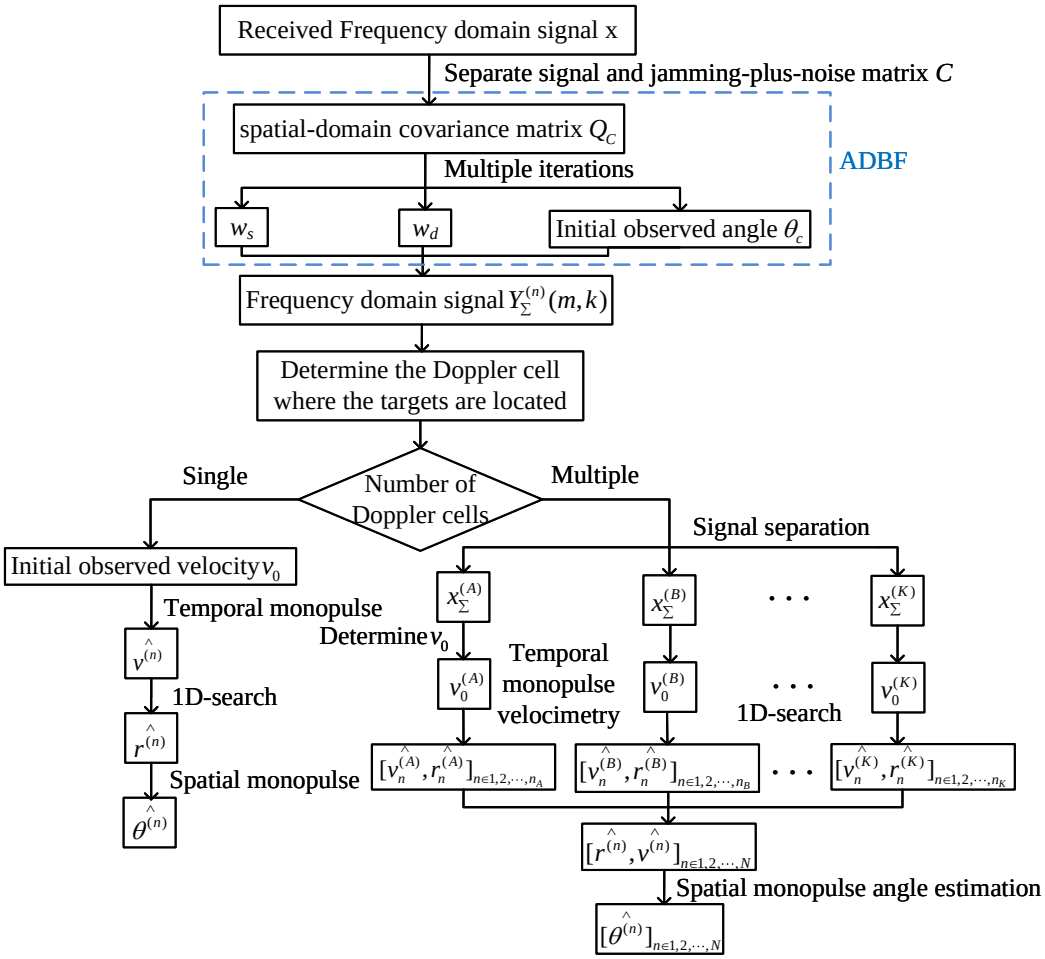

Fig. 4. Flowchart of the proposed AM-STCMP algorithm.

Step 3:

M-STCMP operations are applied to each beam, where $k = A, B, \cdots, K$. For each beam $\mathbf{x}_\Sigma^{(k)}$, the initial observed velocity is denoted by $v_0^{(k)}$. The parameter estimation process for $\left[\hat{v}_n^{(k)}, \hat{r}_n^{(k)}, \hat{\alpha}_n^{(k)}, \hat{\beta}_n^{(k)}\right]_{n\in\{1,2,\cdots,n_k\}}$ is carried out iteratively until the energy of the residual components falls below a predefined noise threshold. Here, n_k denotes the number of targets detected within beam k.

Step 4:

(1) To further refine the initially estimated parameters, an iterative substitution procedure is conducted for each of the N targets. The estimates obtained in Step 3 are denoted as $\left[\hat{r}^{(n)}, \hat{v}^{(n)}, \hat{\alpha}^{(n)}, \hat{\beta}^{(n)}\right]_{n\in\{1,2,\cdots,N\}}$. The initial observed velocities corresponding to the targets are recorded as $\left[v_0^{(n)}\right]_{n\in\{1,2,\cdots,N\}} = \left[\underbrace{v_0^{(A)},\cdots,v_0^{(A)}}_{n_A}, \underbrace{v_0^{(B)},\cdots,v_0^{(B)}}_{n_B}, \cdots, \underbrace{v_0^{(K)},\cdots,v_0^{(K)}}_{n_K}\right]$. The estimated set is denoted as Θ, where $\Theta = \left[\hat{r}^{(n)}, \hat{v}^{(n)}, \hat{\alpha}^{(n)}, \hat{\beta}^{(n)}\right]_{n\in\{1,2,\cdots,N\}}$.

(2) In each iteration, the parameters of the nth target are updated by excluding its current estimates and substituting the remaining N–1 target estimates into (3) and (4) to obtain $\mathbf{Y}_\Sigma^{(n)}$ and $\mathbf{Y}_\Delta^{(n)}$. Then, $\mathbf{Y}_\Sigma^{(n)}$, $\mathbf{Y}_\Delta^{(n)}$ and $v_0^{(n)}$ are substituted into (21)–(24) to obtain $\left[\hat{r}^{(n)}, \hat{v}^{(n)}, \hat{\alpha}^{(n)}, \hat{\beta}^{(n)}\right]$, and the corresponding estimates in Θ are updated.

(3) The procedure of Step 4(2) is repeated until all N targets are updated.

Step 5:

$\left[\hat{\alpha}^{(n)}, \hat{\beta}^{(n)}\right]_{n\in\{1,2,\ldots,N\}}$ is substituted into (26) to obtain the sine estimate of the angle $\left[\hat{u}^{(n)}\right]_{n\in\{1,2,\ldots,N\}}$. The corresponding angle estimate $\left[\hat{\theta}^{(n)}\right]_{n\in\{1,2,\ldots,N\}}$ is then obtained.

In summary, the proposed AM-STCMP algorithm enhances the conventional M-STCMP framework by incorporating an adaptive monopulse technique in the spatial domain. This integration maintains high parameter estimation accuracy even under severe jamming conditions and significantly improves jamming suppression capability.

4. Simulation Results and Analysis

To evaluate the effectiveness of the AM-STCMP algorithm, several simulations were conducted. The simulation parameters are provided in Tab. 1 for reference.

To ensure consistency across experiments, a 21-element linear array, 9 pulses, and linear frequency-modulated signals are used for all targets. The main beam width spans approximately from −3° to 3°. The target signals, noise components, and jamming signals are assumed to be mutually uncorrelated, and the jamming signals are modeled as far-field sources. The RMSE metric is employed to quantitatively evaluate parameter estimation accuracy. Following [13], two simulation scenarios are considered for a systematic comparison with the baseline M-STCMP algorithm: (1) all targets are confined within the same Doppler cell, and (2) the targets are distributed across multiple Doppler cells. For clarity, in the legends, the suffixes 1–3 denote Targets 1–3, respectively; AM-STCMP, M-STCMP, and No Jamming denote the proposed algorithm under jamming, the conventional M-STCMP algorithm under jamming, and the jamming-free M-STCMP case, respectively.

Simulation 1. All targets are distributed within the same Doppler cell. The target parameters are shown in Tab. 2. The JNR is varied with a single jammer located at 6°. Figure 5 compares the parameter estimation performance of the M-STCMP and AM-STCMP algorithms. It displays the RMSEs of velocity, range, and angle, respectively, as functions of the JNR.

Parameter	Value
Bandwidth B	5 MHz
Carrier frequency f_c	1 GHz
Number of array elements N_e	21
Signal wavelength λ	0.3 m
Inter-element spacing d	0.15 m
Pulse width T	20 µs
Pulse repetition frequency PRF	800 Hz
Number of pulses N_p	9

Tab. 1. System simulation parameters.

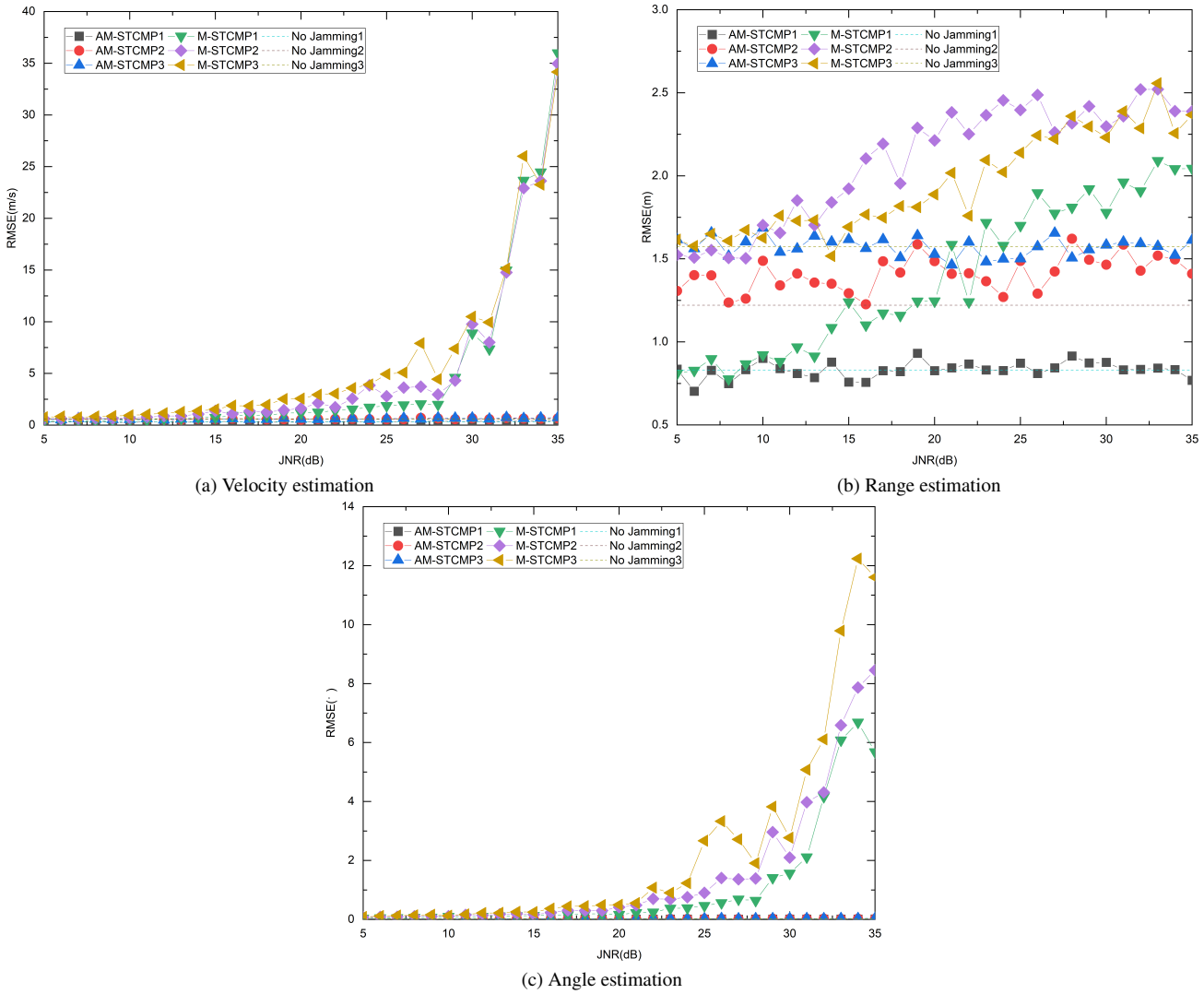

(a) Velocity estimation

(b) Range estimation

(c) Angle estimation

Fig. 5. Comparison of RMSE when targets are located in the same Doppler cell.

Target number	1	2	3
Velocity [m/s]	27.9	25.6	23.7
Doppler cells	7	7	7
Range [m]	351.2	379.4	400.3
Angle [°]	0.5	0.55	0.52
SNR [dB]	20	17	14

Tab. 2. Target information in Simulation 1.

Simulation 1 evaluates the parameter estimation performance of the AM-STCMP and M-STCMP algorithms under jamming conditions and compares them with the performance of the M-STCMP algorithm in a jamming-free environment. The x-axis represents the JNR, ranging from 5 to 35 dB, in increments of 1 dB. At each JNR level, 100 Monte Carlo simulations were performed, and the covariance matrix was estimated using 100 snapshots.

As shown in Fig. 5, the performance of the M-STCMP algorithm in estimating the velocity, range, and angle decreases as the JNR increases. When the JNR exceeds 25 dB, the estimation accuracy declines sharply. The AM-STCMP algorithm maintains strong estimation performance even under relatively high jamming conditions. For Target 1, when the JNR is 35 dB, the AM-STCMP algorithm reduces the RMSEs of velocity, range, and angle by 35.58 m/s, 1.28 m, and 5.66°, respectively, compared with the M-STCMP algorithm. Among the three RMSEs of the M-STCMP algorithm, the range performance remains relatively stable due to the inherent anti-jamming properties of maximum likelihood estimation. In contrast, the velocity performance decreases most significantly, as excessive jamming severely degrades the accuracy of the observed velocity values. Additionally, the dotted line in the figure represents the performance of the M-STCMP algorithm with an SNR of 20 dB and no jamming. Comparing this curve with the AM-STCMP results shows that the proposed algorithm achieves performance comparable to that of the M-STCMP algorithm under jamming-free conditions, confirming the effectiveness of the AM-STCMP algorithm.

Simulation 2. The targets are distributed across multiple Doppler cells, and the target parameters are provided in Tab. 3. The JNR is varied with a single jamming source at an arrival direction of 6°. The JNR ranges from 5 to 35 dB. Figure 6 compares the parameter estimation performance of

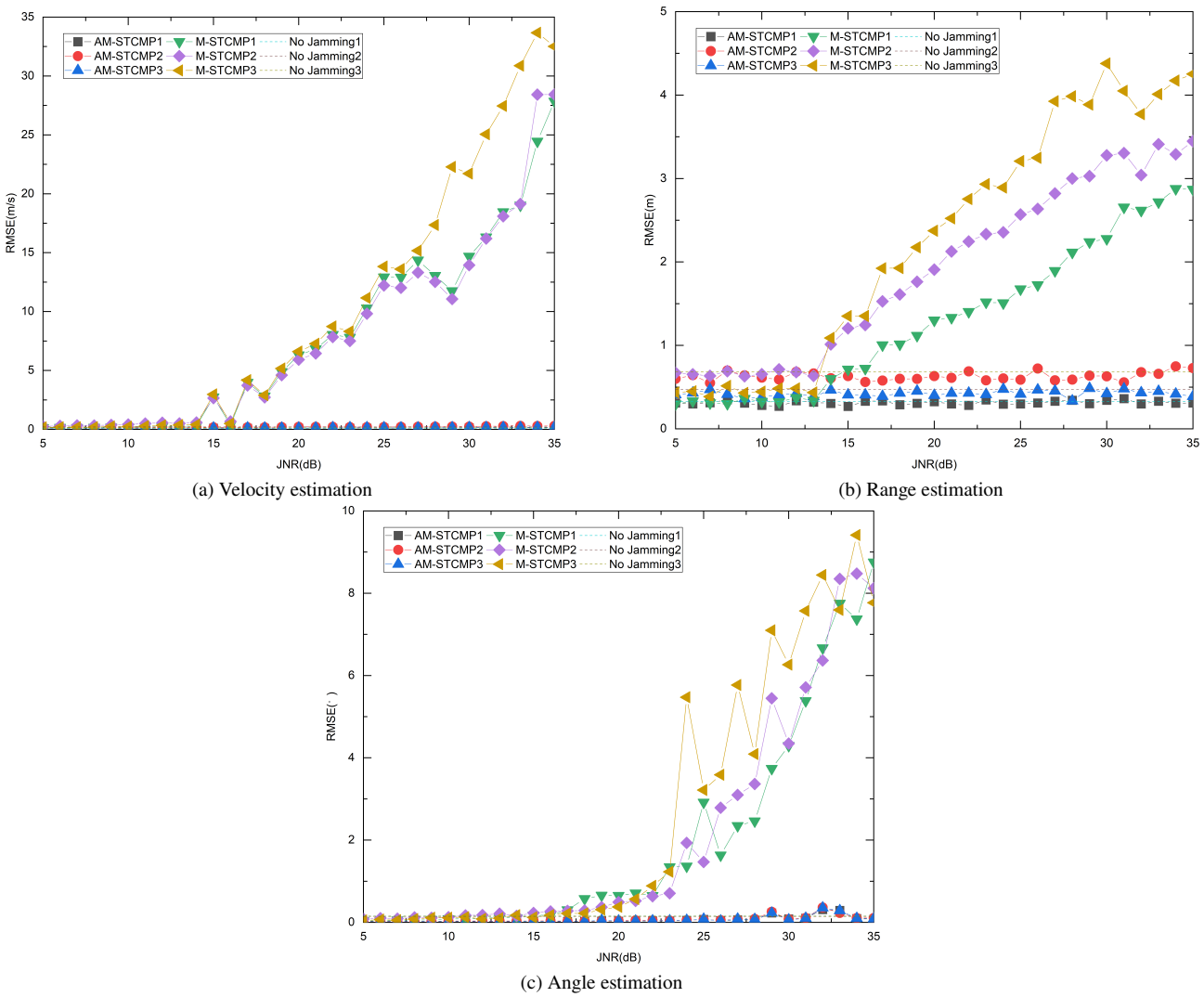

(a) Velocity estimation

(b) Range estimation

(c) Angle estimation

Fig. 6. Comparison of RMSE when targets are located in different Doppler cells.

the M-STCMP and AM-STCMP algorithms under jamming conditions, as well as that of the M-STCMP algorithm under jamming-free conditions. It displays the RMSE as a function of JNR for velocity, range, and angle, respectively.

In Simulation 2, 100 Monte Carlo simulations were performed at each JNR level, with the covariance matrix estimated via 100 snapshots. The x-axis of the simulation graph represents the JNR. Under low JNR conditions, the two algorithms exhibited comparable performance due to the relatively high SNR. The maximum likelihood and monopulse algorithms inherent to the M-STCMP algorithm possess certain anti-jamming capabilities, making them less susceptible to jamming when it is minimal. As with Simulation 1, the proposed algorithm demonstrates superior performance in the velocity, range, and angle estimation as the JNR increases, compared with the conventional M-STCMP algorithm. The most significant improvement is in the estimation of velocity, which is particularly susceptible to errors in the presence of jamming and noise. The dotted line in the figure represents the performance of the M-STCMP algorithm with an SNR of 20 dB and no jamming, similar to Simulation 1. The performance of the proposed algorithm is comparable to that of the M-STCMP algorithm under jamming-free conditions, confirming the effectiveness of the AM-STCMP algorithm.

When comparing Simulation 1 and Simulation 2, the overall parameter estimation performance in Simulation 2 is superior to that of Simulation 1. This improvement is due to the separation of signals in the Doppler cells, which allows for the isolation of multiple targets located within the same range resolution cell. As a result, the number of targets within each Doppler cell is reduced, effectively minimizing jamming from targets in other Doppler cells and thereby improving estimation accuracy.

Target number	1	2	3
Velocity [m/s]	11.9	41.3	13.8
Doppler cells	7	9	7
Range [m]	350.4	379.4	401.1
Angle [°]	0.5	0.52	0.55
SNR [dB]	20	17	14

Tab. 3. Target information in Simulation 2.

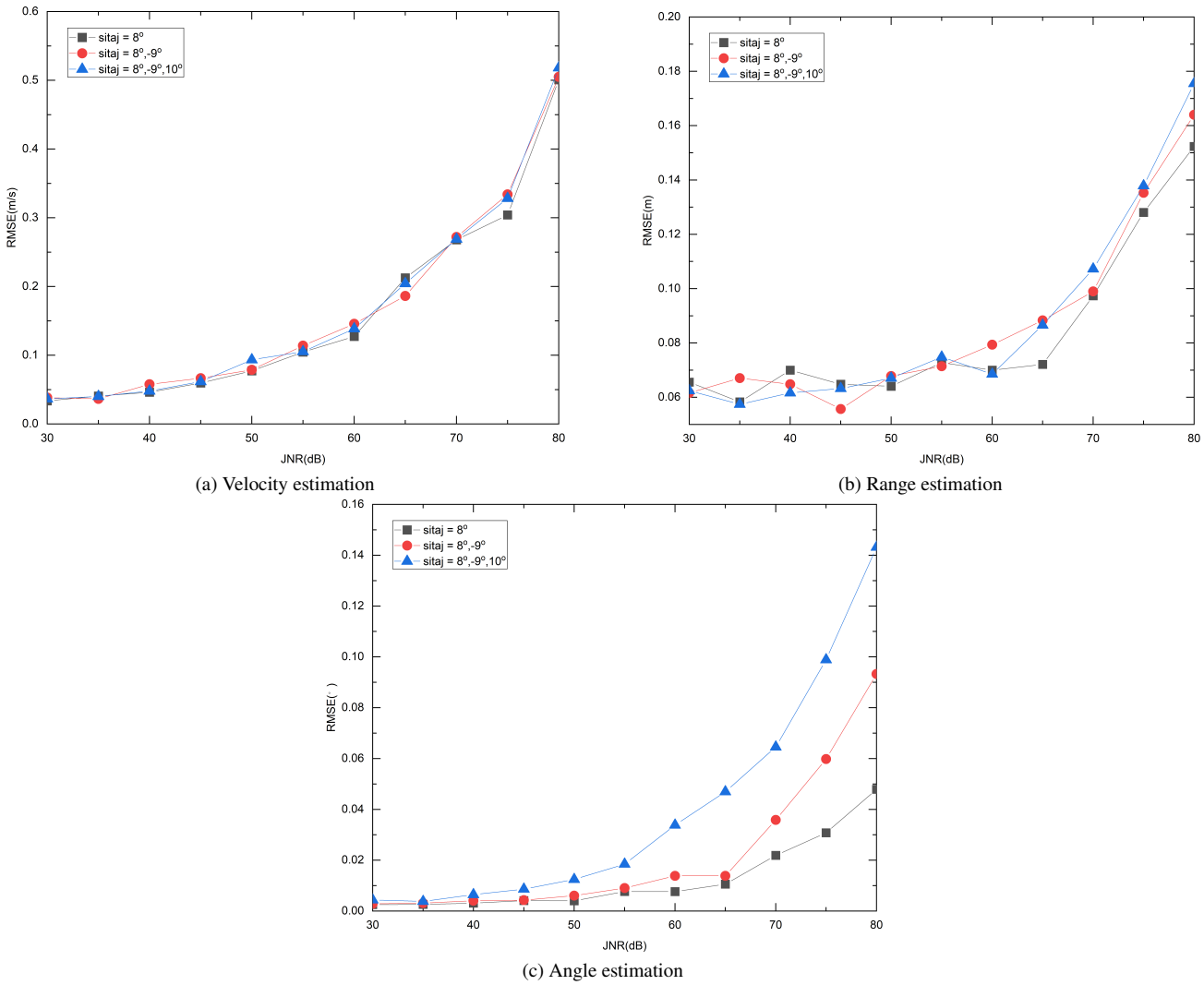

(a) Velocity estimation

(b) Range estimation

(c) Angle estimation

Fig. 7. The impact of the number of jamming sources on algorithm estimation performance.

Number of jamming sources	1	2	3
Jamming angle [°]	8	8, −9	8, −9, 10

Tab. 4. Jammer configuration in Simulation 3.

The two simulations show minor fluctuations due to the limited number of Monte Carlo iterations, but the overall trend of the curves is unaffected, ensuring a valid comparison of the two algorithms' performance. The simulations demonstrate the effectiveness of the proposed algorithm in jamming environments. To further analyze the performance of the proposed algorithm, additional simulations were conducted in different jamming environments.

Simulation 3. The parameters for the jamming environment are provided in Tab. 4. In Simulation 3, one target is considered. The SNR is set to 20 dB, with a range of 351.2 m, a velocity of 27.9 m/s, and an angle of 1.5°. This simulation analyzes the impact of varying the number of jamming sources on the performance of the proposed algorithm. Figure 7 displays the RMSEs of the velocity, range, and angle, respectively, as a function of JNR. To prevent mainlobe jamming from unduly affecting the analysis, sidelobe jamming is considered, with an arrival direction close to that of the target.

As shown in Fig. 7, increasing the number of jamming sources significantly degrades estimation performance, leading to decreased overall accuracy. Consistent with previous simulations, range estimation is less affected by jamming than velocity and angle estimation, due to the inherent anti-jamming properties of the maximum likelihood algorithm. Furthermore, the performance under a single jamming source demonstrates that the AM-STCMP algorithm remains robust even at a JNR of 80 dB, verifying the effectiveness of the proposed method.

5. Conclusion

To address the limited jamming resistance of the conventional M-STCMP algorithm, this study proposes the AM-STCMP algorithm. The proposed solution integrates spatial monopulse processing with ADBF techniques to dynamically optimize the sum and difference channel weight vectors for target signals. This adaptive optimization significantly improves anti-jamming capability while maintaining estimation accuracy. Comprehensive simulation results demonstrate that, in complex jamming environments, the AM-STCMP algorithm achieves parameter estimation performance comparable to that of the conventional M-STCMP algorithm under jamming-free conditions.

Acknowledgments

This work was supported by the National Natural Science Foundation of China under Grant 62271190.

References

[1] NICKEL, U., CHAUMETTE, E., LARZABAL, P. Estimation of extended targets using the generalized monopulse estimator: Extension to a mixed target model. *IEEE Transactions on Aerospace and Electronic Systems*, 2013, vol. 49, no. 3, p. 2084–2096. DOI: 10.1109/TAES.2013.6558043

[2] CAI, F., FAN, H., SONG, Z., et al. Difference beam aided target detection in monopulse radar. *Chinese Journal of Aeronautics*, 2015, vol. 28, no. 5, p. 1485–1493. DOI: 10.1016/j.cja.2015.08.007

[3] SCHMIDT, R. Multiple emitter location and signal parameter estimation. *IEEE Transactions on Antennas and Propagation*, 1986, vol. 34, no. 3, p. 276–280. DOI: 10.1109/TAP.1986.1143830

[4] LIU, R., ZHANG, J., JI, Y., et al. Multibeam generalized monopulse angle estimation for APAR. *IEEE Sensors Journal*, 2024, vol. 24, no. 24, p. 41311–41322. DOI: 10.1109/JSEN.2024.3482702

[5] SHERMAN, S. M. Complex indicated angles applied to unresolved radar targets and multipath. *IEEE Transactions on Aerospace and Electronic Systems*, 1971, vol. 7, no. 1, p. 160–170. DOI: 10.1109/TAES.1971.310264

[6] BLAIR, W. D., BRANDT-PEARCE, M. Monopulse DOA estimation of two unresolved Rayleigh targets. *IEEE Transactions on Aerospace and Electronic Systems*, 2001, vol. 37, no. 2, p. 452–469. DOI: 10.1109/7.937461

[7] SINHA, A., KIRUBARAJAN, T., BAR-SHALOM, Y. Maximum likelihood angle extractor for two closely spaced targets. *IEEE Transactions on Aerospace and Electronic Systems*, 2002, vol. 38, no. 1, p. 183–203. DOI: 10.1109/7.993239

[8] ZHENG, Y., TSENG, S., YU, K. Closed-form four-channel monopulse two-target resolution. *IEEE Transactions on Aerospace and Electronic Systems*, 2003, vol. 39, no. 3, p. 1083–1089. DOI: 10.1109/TAES.2003.1238760

[9] GINI, F., GRECO, M., FARINA, A. Multiple radar targets estimation by exploiting induced amplitude modulation. *IEEE Transactions on Aerospace and Electronic Systems*, 2003, vol. 39, no. 4, p. 1316–1332. DOI: 10.1109/TAES.2003.1261131

[10] GRECO, M., GINI, F., FARINA, A. Joint use of sum and delta channels for multiple radar target DOA estimation. *IEEE Transactions on Aerospace and Electronic Systems*, 2007, vol. 43, no. 3, p. 1146–1154. DOI: 10.1109/TAES.2007.4383604

[11] FU, M., GAO, C., LI, Y., et al. Monopulse-radar angle estimation of multiple targets using multiple observations. *IEEE Transactions on Aerospace and Electronic Systems*, 2021, vol. 57, no. 2, p. 968–983. DOI: 10.1109/TAES.2020.3035434

[12] LI, N., HU, X. Ultrawideband mutual RFI mitigation between SAR satellites: From the perspective of European Sentinel-1A. *IEEE Transactions on Geoscience and Remote Sensing*, 2024, vol. 62, p. 1–20. DOI: 10.1109/TGRS.2024.3501309

[13] ZHANG, Y., SHEN, M., WU, D., et al. Reduced complexity multiple-target angle-Doppler-range estimation using space-time cascaded monopulse processing. *Digital Signal Processing*, 2023, vol. 143, p. 1–10. DOI: 10.1016/j.dsp.2023.104239

[14] TAN, M., GONG, J., WANG, C. Range dimensional monopulse approach with FDA-MIMO radar for mainlobe deceptive jamming suppression. *IEEE Antennas and Wireless Propagation Letters*, 2024, vol. 23, no. 2, p. 643–647. DOI: 10.1109/LAWP.2023.3331573

[15] SHI, Y., HUANG, L., QIAN, C., et al. Shrinkage linear and widely linear complex-valued least mean squares algorithms for adaptive beamforming. *IEEE Transactions on Signal Processing*, 2015, vol. 63, no. 1, p. 119–131. DOI: 10.1109/TSP.2014.2367452

[16] QIAN, H., LIU, K., WANG, W. Shrinkage widely linear recursive least square algorithms for beamforming. *IEICE Transactions on Communications*, 2016, vol. E99.B, no. 7, p. 1532–1540. DOI: 10.1587/transcom.2015EBP3322

[17] WU, H., LIU, R., GUO, Y., et al. Performance analysis of mainlobe canceller for monopulse at subarray level in the presence of amplitude-phase error. *IEEE Transactions on Aerospace and Electronic Systems*, 2024, vol. 60, no. 2, p. 2461–2473. DOI: 10.1109/TAES.2024.3354224

[18] XIONG, Y., XIE, W. Adaptive iterative monopulse estimation method based on space-time constraint. (in Chinese) *Systems Engineering and Electronics*, 2022, vol. 44, no. 8, p. 2506–2514. DOI: 10.12305/j.issn.1001-506X.2022.08.15

[19] WARD, J. Maximum likelihood angle and velocity estimation with space-time adaptive processing radar. In *Conference Record of The Thirtieth Asilomar Conference on Signals, Systems and Computers*. Pacific Grove (CA, USA), 1996, vol. 2, p. 1265–1267. DOI: 10.1109/ACSSC.1996.599148

[20] NICKEL, U. Monopulse estimation with adaptive arrays. *IEE Proceedings F (Radar and Signal Processing)*, 1993, vol. 140, no. 5, p. 303–308. DOI: 10.1049/ip-f-2.1993.0042

About the Authors . . .

Ling QIAO was born in 1997. She received the M.S. degree in Electronic and Communication Engineering from Nanjing University of Posts and Telecommunications, Nanjing, China. She is currently pursuing the Ph.D. degree in Information and Communication Engineering with Hohai University, China. Her research interests include radar signal processing and moving target parameter estimation.

Mingwei SHEN (corresponding author) was born in 1981. He received the Ph.D. degree in Electronic Engineering from Nanjing University of Aeronautics and Astronautics (NUAA), Nanjing, China. He is currently a Professor with Hohai University, China. His research interests include space-time adaptive processing (STAP) and radar moving target detection.

Ruiyan CHEN was born in 2000. She received the M.S. degree in Electronic Science and Technology from Hohai University, Nanjing, China. Her research interests include array signal processing.

Yongshu ZHANG was born in 1999. She received the M.S. degree in Electronic Science and Technology from Hohai University, China. Her research interests include array signal processing.

Di WU was born in 1982. He received the Ph.D. degree in Communication and Information Systems from Nanjing University of Aeronautics and Astronautics (NUAA), Nanjing, China. He is currently a Professor with NUAA. His research interests include radar imaging algorithms, space-time adaptive processing (STAP), and synthetic aperture radar ground moving target indication (SAR/GMTI).

Daiyin ZHU was born in 1974. He received the Ph.D. degree in Electronics from Nanjing University of Aeronautics and Astronautics (NUAA), Nanjing, China. He is currently a Professor with NUAA. His research interests include radar imaging algorithms, synthetic aperture radar ground moving target indication (SAR/GMTI), synthetic aperture radar (SAR)/ inverse synthetic aperture radar (ISAR) autofocus techniques, SAR interferometry, and multiple-input multiple-output (MIMO) SAR signal processing.